Progress In Electromagnetics Research C, Vol. 136, 61–74, 2023

Study of SAR Data and Spatial Distribution in a Peace Lily Plant Model under Different Electromagnetic Exposure Scenarios

Nibedita Mukherjee[1], Ardhendu Kundu[2, *], and Monojit Mitra[3]

Abstract—Over the last three decades, the presence of electromagnetic radiation in the open environment has increased by many folds due to wide utilization of cellular data and voice communication over multiple wireless communication bands. Thus with the increased utilization of electromagnetic energy, several global as well as national electromagnetic exposure regulatory norms have been put in effect across geographical boundaries to safeguard humans from immediate effects of Radio Frequency radiation. Specific Absorption Rate (SAR) quantification is well established in literature to measure the rate of electromagnetic energy absorption by living objects (humans as well as plants) while external microwaves impinge on them. It should also be considered that plants do absorb fairly reasonable amount of electromagnetic energy mainly from cell tower and Wi-Fi antennas owing to high permittivity (ε'_r) and conductivity (σ) of constituent tissues. However, it is indeed unfortunate that worldwide there are very limited concerns regarding electromagnetic energy absorptions in plants, fruits, and flowers — thus, no electromagnetic exposure regulatory guidelines have yet been put in effect to safeguard plants, crops, fruits, and flowers. Thus, it is absolutely necessary to quantify microwave energy absorption rates in various fruit, flower, and plant models due to electromagnetic radiations from different sources. Later on, consequent biological responses in plants along with associated effects on ecosystem and fruit nutrition value should be investigated. With this motivation, electromagnetic energy absorption rates, i.e., SAR values along with associated spatial distributions, have been estimated in this article for a typical Peace Lily (*Spathiphyllum wallisii*) plant model considering different frequencies of exposure, directions of plane wave incidence, and polarizations of incident wave. Peace Lily plant has been chosen for this investigation as it is known for air purifying capability and indoor usage — furthermore, the plant parts can be easily characterized and modelled for electromagnetic simulations. Plants are of asymmetric shapes with varied sizes. To represent the typical geometric shape considering the most practical observation, a three dimensional Peace Lily plant model has been designed using CST Microwave Studio electromagnetic solver. The model has been exposed to linearly polarized plane waves at three distinct frequencies (947.50 MHz, 1842.50 MHz, and 2450 MHz) following Indian electromagnetic exposure regulatory guidelines — these frequencies are used for voice, data or Wi-Fi communications. Dielectric properties (ε_r), i.e., permittivity (ε'_r) as well as loss tangent ($\tan\delta$) of different peace lily plant tissues, have been characterized over a broad frequency band employing open ended coaxial probe measurement technique. Measured tissue dielectric properties (ε_r) have been fitted to the developed plant model to evaluate SAR data and spatial distributions. At each frequency, significant variations have been noted in magnitudes and positions of Maximum Local Point SAR (MLP SAR), 1 g averaged SAR, and 10 g averaged SAR values for six different combinations of direction of arrival and incident wave polarization. Observations indicate different orders of change in MLP SAR, 1 g averaged SAR, and 10 g averaged SAR values in the plant model even for same combination of frequency of exposure, power density, direction of arrival (plane wave), and polarization of incident wave. Data reported in this article can be considered as reference to investigate consequent physiological or molecular responses in plants and revise electromagnetic exposure regulatory policies to protect plants and the entire ecosystem.

Received 21 May 2023, Accepted 10 July 2023, Scheduled 11 August 2023

* Corresponding author: Ardhendu Kundu (ardhendukundu.1989@gmail.com).

[1] Electronics and Communication Engineering Department, Budge Budge Institute of Technology, Budge Budge, India. [2] Electronics and Telecommunication Engineering Department, Jadavpur University, Kolkata, India. [3] Department of Electronics and Telecommunication Engineering, IIEST, Shibpur, Howrah, India.

1. INTRODUCTION

Radio Frequency (RF) electromagnetic energy is being utilized over a number of frequency bands for uninterrupted wireless connectivity to support voice and data services. It is well known that all living objects including humans and plants are exposed to electromagnetic radiation. Therefore, it is important to investigate electromagnetic energy absorption rates in humans as well as plants along with consequent biological effects. Most human and plant biological tissues possess reasonably high dielectric properties (ε_r), i.e., permittivity (ε'_r) as well as loss tangent ($\tan\delta$) due to the presence of sufficient water and ion contents [1–7]. Electromagnetic energy absorption rate in human equivalent phantom models has been quantified in terms of 'Specific Absorption Rate (SAR)' over last four decades [8–16]. SAR is quantified as electromagnetic energy absorption rate per unit mass of biological tissue while an external RF wave impinges on it and then passes through with reduced strength — in general, it is expressed as W/kg or mW/g. Furthermore, a number of articles report electromagnetic irradiation induced biological responses in humans and consequent health effects [17–26]. However to protect the entire ecosystem adopting a sustainable approach, electromagnetic energy absorption rates and the associated plant responses should also be probed. In the last decade, SAR data and spatial distributions have also been investigated for a limited number of fruit and plant models [27–34]. It has been observed that the SAR values are quite significant in those fruit and plant prototypes. Moreover, plant structures are asymmetric in nature — hence, SAR values and spatial distributions are expected to alter with different directions of wave propagation and wave polarizations. Thus, in this article, SAR data and associated spatial distributions have been reported for a typical Peace Lily plant (*Spathiphyllum wallisii*) model. At first, complex dielectric properties (ε_r), i.e., permittivity (ε'_r) as well as loss tangent ($\tan\delta$) data over a broad frequency range, have been measured for Peace Lily flower, leaf as well as stem specimens employing open ended coaxial probe characterization technique [35–39]. Next, frequency specific complex tissue dielectric properties (ε_r) have been fitted to the developed Peace Lily plant model in CST Microwave Studio (CST MWS) electromagnetic solver for simulations [40]. Once the model has been analyzed using Time Domain (TD)/transient solver, SAR data along with spatial distributions have been reported for six distinct combinations of plane wave propagation and incident wave polarization at three separate frequencies, i.e., 947.50 MHz, 1842.50 MHz, and 2450.00 MHz, respectively — these frequencies are mainly transmitted for cellular voice, data or Wi-Fi communications. Altogether 72 SAR data have been reported for the designed Peace Lily plant model after 18 simulations as per existing Indian electromagnetic exposure guidelines [41]. Simulated results demonstrate wide variation in SAR data due to the change in either direction of propagation or polarization of incident plane wave (even at a particular frequency of operation). Furthermore, it should be taken into note that the position of maximum SAR value also changes along with magnitude due to the change in the direction of propagation or polarization of incident wave [31, 34].

2. EXISTING INDIAN ELECTROMAGNETIC REGULATORY STANDARDS

With the widespread utilization of wireless electromagnetic spectrum, a number of global as well as national electromagnetic exposure regulatory standards have been prescribed worldwide to protect humans [41–46]. Among them, electromagnetic standards prescribed by International Commission on Non-Ionizing Radiation Protection (ICNIRP) and Federal Communications Commission (FCC) have been adopted widely across geographical boundaries [42, 43]. In addition, a number of countries such as Switzerland, Russia, Italy, and India have adopted stringent national electromagnetic standards [41, 44–46]. In India, prescribed electromagnetic regulatory standards (reference power density) have been made 10 times stricter than ICNIRP standards [41, 42]. It is evident that these international as well as national electromagnetic regulatory standards indeed lack uniformity in terms of prescribed reference power density and SAR limits for humans [41–48]. To date, there is no clause in these guidelines in particular to protect plants, fruits, and flowers from potential effects of electromagnetic radiation. In this work, the current Indian electromagnetic exposure regulations for general public coverage have been considered for SAR simulations in the Peace Lily plant model — as, in the current scenario, all plants are exposed to electromagnetic radiation in accordance with the active Indian electromagnetic exposure regulatory standards for protecting public. The prescribed reference power density limits for

Table 1. Power density and electric field as per Indian electromagnetic exposure regulatory standards [41].

Public electromagnetic exposure standards in India	Frequency (MHz)		
	947.50	1842.50	2450
Power density (W/m^2)	0.474	0.921	1.00
Peak electric field (V/m)	18.90	26.35	27.46

Indian public coverage and equivalent electric field values are summarized in Table 1 [41].

3. MEASURED DIELECTRIC PROPERTIES AND MATERIAL DENSITIES OF PEACE LILY SPECIMENS

Permittivity (ε_r') of a material is defined by its capability to store incident electric field energy whereas electrical conductivity (σ)/loss tangent ($\tan\delta$) is associated with the fractional amount of stored energy that gets converted to heat or any other form. Biological tissues in general possess high permittivity (ε_r') as well as loss tangent ($\tan\delta$) over a broad range of frequency spectrum [5–7, 27–34]. There are several standard measurement techniques for material dielectric properties (ε_r) characterization — among them, the measurement technique employing open ended coaxial probe is the most convenient one for dielectric properties (ε_r) characterization of different biological tissues [5–7, 27–39]. Thus the same technique has been adopted to characterize broadband complex dielectric properties (ε_r) of Peace Lily specimens.

This particular measurement technique characterizes tissue dielectric properties (ε_r) by measuring phase and amplitude of the reflected electromagnetic signal at open end of the coaxial probe where the probe is firmly positioned on the flat sample surface and immersed inside in the case of a liquid specimen. The coaxial probe is integrated with a Vector Network Analyzer (VNA) for measuring reflection coefficient data over broad frequency spectrum. The open ended coaxial probe is modelled with a parallel combination of two fringing capacitances from inner to outer conductor through biological tissue and through the intervening dielectric material (Teflon in most cases) along with a radiation conductance between inner and outer conductors through biological tissue specimen. These parameter values largely depend upon permittivity (ε_r') as well as conductivity (σ) of biological specimen under test, frequency of operation, and probe dimensions. Overall input admittance of an open ended coaxial probe is complex — radiation conductance and fringing capacitance parameters are associated with the permittivity (ε_r') and conductivity (σ) of complex tissue dielectric properties (ε_r). Detailed mathematical analyses are by now available in literature [30, 35–39].

Commercially available 85070E open ended coaxial probe kit and E5071B Vector Network Analyzer (manufactured by Agilent Technologies) have been utilized to characterize broadband dielectric properties (ε_r) of Peace Lily specimens at normal room temperature (refer to Figs. 1(a), (b), and (c)) — dielectric properties (ε_r) have been characterized up to a range of 8.5 GHz. The measured permittivity (ε_r') as well as loss tangent ($\tan\delta$) data at 947.50 MHz, 1842.50 MHz, and 2450 MHz are summarized in Table 2.

Table 2. Measured complex dielectric properties of Peace Lily plant specimens.

Peace Lily Specimen	*Dielectric Properties*	*Frequency of Interest*		
		947.50 MHz	1842.50 MHz	2450 MHz
Flower	Permittivity	56.32	53.82	53.64
	Loss Tangent	0.297	0.232	0.245
Leaf	Permittivity	29.70	28.20	28.23
	Loss Tangent	0.289	0.229	0.230
Stem	Permittivity	25.73	24.30	24.48
	Loss Tangent	0.315	0.244	0.251

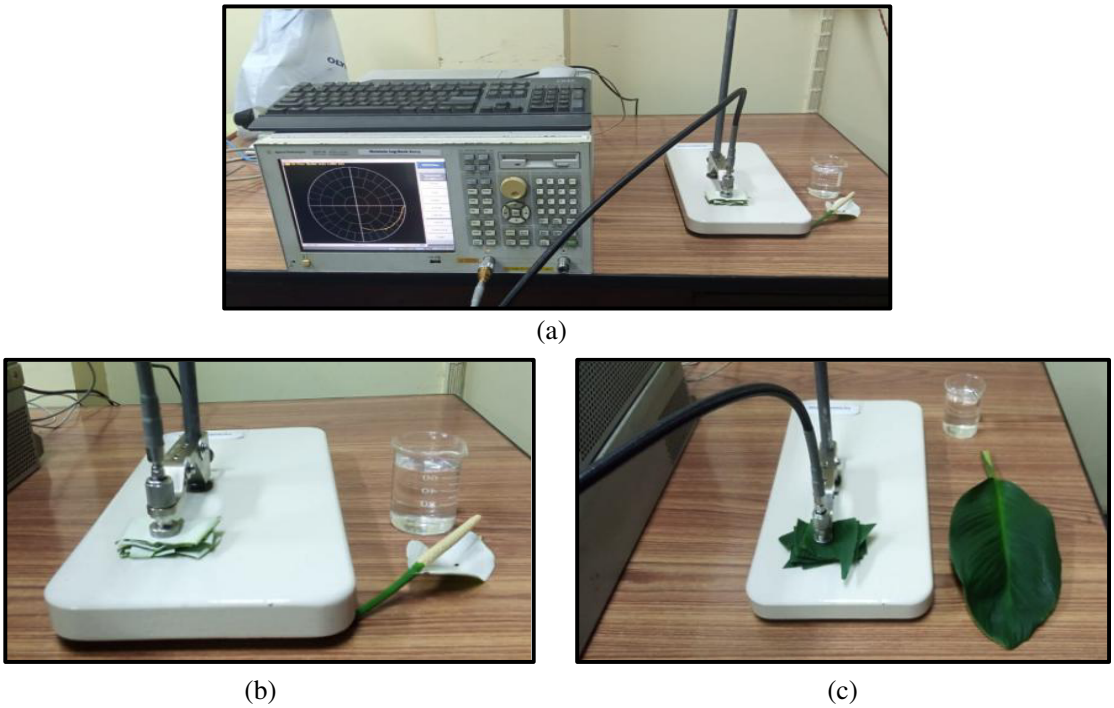

(a) (b) (c)

Figure 1. (a), (b), (c) Dielectric properties test setup for Peace Lily plant specimens.

Material density of Peace Lily flower, leaf, and stem specimens is necessary for SAR computation. Mass and volume of individual Peace Lily specimens have been calculated using an electronic balance, a glass beaker, a stone, and a cotton string. Measured densities for Peace Lily flower, leaf, and stem are 1180, 707.50, and 707.50 $\mathrm{kg/m^3}$, respectively.

4. THREE DIMENSIONAL DESIGN OF A TYPICAL PEACE LILY PLANT MODEL AND SAR SIMULATION SETUP

A typical Peace Lily plant model containing three leaves and one flower along with associated stems has been designed in CST MWS [40]. Both the leaves and flower petal are fairly thin which have been modelled considering the most realistic scenario. The final Peace Lily plant model possesses 36.8 g mass in total — the model is illustrated in Fig. 2. In this model, Peace Lily flower, leaves, and stems have been assigned respective frequency dependent dielectric properties (ε_r) (i.e., permittivity (ε'_r) as well as loss tangent ($\tan\delta$)) along with material densities. In the designed plant prototype, the leaves are of different sizes whereas the flower is standing vertical — please refer to Fig. 2. Hence, the entire plant structure is asymmetric. In simulation setup, transient solver has been selected due to the complex geometrical shape of the plant structure along with lossy low quality factor of plant tissue layers — thus, a robust meshing has been achieved for the designed plant model. The time domain/transient solver available in CST MWS was developed using a numerical computation scheme called Finite Integration Technique (FIT) — this scheme was first developed in 1977 [49, 50]. The plant model is spatially discretized in hexahedral shape meshes of different sizes. Furthermore, one wavelength spatial length in biological tissue is divided in 20 segments. In the simulation settings, four Perfectly Matched Layers (PMLs) have been utilized as the electromagnetic absorbing boundary where separation from the plant model to absorbing boundary (PML) has been maintained at 0.10 cm. For reaching the steady state energy criterion, -40 dB inverse transformation accuracy has been selected for observing the frequency domain characteristics [32–40]. Linearly polarized plane waves at individual frequencies have been impinged on the Peace Lily plant model with six distinct combinations of direction of wave propagation and incident wave polarization in six separate simulation runs. Once all six simulations have been completed at a particular frequency, disparity in spatial coordinate location and magnitude

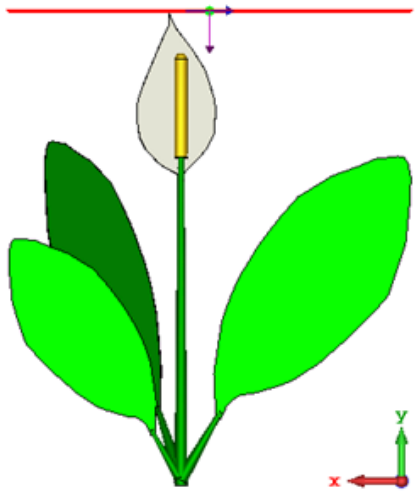

Figure 2. A typical Peace Lily plant model designed in CST Microwave Studio.

of maximum SAR data have been noted for the Peace Lily plant model. Point SAR inside a mesh-cell is estimated employing the formula $\sigma|E|^2/2\rho$ — here, σ, E, and ρ are plant tissue conductivity, peak value of electric field at the point of SAR calculation, and plant tissue density. IEEE/IEC 62704-1 SAR averaging technique has been utilized in CST MWS to calculate SAR data [32, 40, 51]. To be specific, SAR simulations have been performed at three frequencies of interest, i.e., 947.50 MHz, 1842.50 MHz, and 2450 MHz in accordance with the existing Indian electromagnetic exposure regulatory standards. In this article, recorded Maximum Local Point SAR (MLP SAR), 1 g averaged SAR, 10 g averaged SAR, and Whole Body Averaged SAR (WBA SAR) data have been presented at all three frequencies in Indian scenario [41].

5. SAR DATA AND ANALYSES

Discrepancies in MLP SAR, 1 g SAR, 10 g SAR, and WBA SAR data due to six distinct combinations of direction of propagation and incident wave polarization have been summarized at all three frequencies — please refer to Table 3 to Table 5. Maximum SAR values along with respective location coordinates

Table 3. SAR data variation for different directions of arrival and incident wave polarizations at 947.50 MHz.

Frequency = 947.50 MHz							
Direction of Propagation & Wave Polarization	**MLP SAR (W/kg)**	**Position [x, y, z] (cm)**	**1g SAR (W/kg)**	**Position [x, y, z] (cm)**	**10g SAR (W/kg)**	**Position [x, y, z] (cm)**	**WBA SAR (W/kg)**
DoP: x= 1 E-field: y axis	0.3370	1.25, 249.5, 1.25	0.1535	-3.75, 286.318, 3.75	0.10203	-57, 183, 1.25	0.09408
DoP: x= -1 E-field: y axis	0.3323	-1.25, 249.5, 1.25	0.1521	-3.75, 286.318, 3.75	0.10258	-57, 183, 1.25	0.09445
DoP: y= -1 E-field: x axis	0.1009	-33, 58.5, 1.25	0.0762	-106.667, 128.75, 1.25	0.04663	-163.25, 158.25, 1.25	0.03217
DoP: y= -1 E-field: z axis	0.0807	102.563, 183, 143.63	0.0340	23.4375, 103.125, 34.1498	0.02970	91.875, 154.75, 134.445	0.01521
DoP: z= 1 E-field: x axis	0.1026	-33, 58.5, 1.25	0.0711	-103, 131.813, 1.25	0.04382	-166.25, 166.875, 1.25	0.03041
DoP: z= -1 E-field: x axis	0.0985	-33, 58.5, 1.25	0.0716	-80, 154.75, 1.25	0.04408	-166.25, 166.875, 1.25	0.03034
Max-to-Min SAR Ratio	**4.18**		**4.51**		**2.34**		**6.21**

Table 4. SAR data variation for different directions of arrival and incident wave polarizations at 1842.50 MHz.

Frequency = 1842.50 MHz							
Direction of Propagation & Wave Polarization	**MLP SAR (W/kg)**	**Position [x, y, z] (cm)**	**1g SAR (W/kg)**	**Position [x, y, z] (cm)**	**10g SAR (W/kg)**	**Position [x, y, z] (cm)**	**WBA SAR (W/kg)**
DoP: x= 1 E-field: y axis	1.3099	1.875, 249.5, 0.625	0.55030	33, 118.75, 0.625	0.426676	-145.75, 131.208, 0.625	0.273455
DoP: x= -1 E-field: y axis	1.3771	-28.955, 57.75, 0.625	0.45466	-26.955, 91.875, 0.625	0.358214	-71.5, 193.875, 0.625	0.2661
DoP: y= -1 E-field: x axis	0.4494	-5.83333, 22.7679, 0.625	0.38268	-82, 79, 0.625	0.164669	-163.833, 160.625, 0.625	0.122003
DoP: y= -1 E-field: z axis	0.3089	105.656, 223.539, 149.29	0.18212	36.5265, 77, 53.6527	0.118479	89.625, 162.187, 127.17	0.05384
DoP: z= 1 E-field: x axis	0.5688	-30.5, 57.75, 0.625	0.31258	79.6875, 168.375, 0.625	0.125554	-172, 185.875, 0.625	0.098936
DoP: z= -1 E-field: x axis	0.5450	-30.5, 57.75, 0.625	0.32969	77.55, 168.375, 0.625	0.127589	-168.75, 175.125, 0.625	0.098077
Max-to-Min SAR Ratio	**4.46**		**3.02**		**3.60**		**5.08**

Table 5. SAR data variation for different directions of arrival and incident wave polarizations at 2450 MHz.

Frequency = 2450 MHz							
Direction of Propagation & Wave Polarization	**MLP SAR (W/kg)**	**Position [x, y, z] (cm)**	**1g SAR (W/kg)**	**Position [x, y, z] (cm)**	**10g SAR (W/kg)**	**Position [x, y, z] (cm)**	**WBA SAR (W/kg)**
DoP: x= 1 E-field: y axis	3.5525	-29.3088, 57.75, 0.625	0.80059	53.625, 150.469, 0.625	0.597119	-157.5, 165.938, 0.625	0.36613
DoP: x= -1 E-field: y axis	2.1832	17.2043, 60.5, 24.3969	0.69924	98.25, 117.5, 0.625	0.396911	45.0938, 105.937, 63.722	0.331692
DoP: y= -1 E-field: x axis	1.7011	-5.66667, 20.7237, 0.625	0.68328	-74.125, 75.25, 0.625	0.273454	-171.5, 185.875, 0.625	0.225614
DoP: y= -1 E-field: z axis	0.5589	28.875, 73.75, 40.6694	0.33499	40.4937, 76.6667, 58.2979	0.205284	96.5625, 160.625, 136.498	0.092563
DoP: z= 1 E-field: x axis	0.8742	-5.66667, 20.7237, 0.625	0.42763	101.325, 94.6875, 0.625	0.182679	-172.5, 195.9, 0.625	0.161569
DoP: z= -1 E-field: x axis	1.1409	22.875, 43.5, 0.625	0.43316	-150.7, 214.083, 0.625	0.175386	-171.5, 185.875, 0.625	0.161483
Max-to-Min SAR Ratio	**6.36**		**2.39**		**3.40**		**3.96**

at 947.50 MHz, 1842.50 MHz, and 2450 MHz have been summarized in Table 3 to Table 5, respectively. Furthermore, the tabulated variations in MLP SAR, 1 g SAR, 10 g SAR, and WBA SAR data are also illustrated in Figs. 4(a) to 4(c), Figs. 5(a) to 5(c), Figs. 6(a) to 6(c), and Fig. 7, respectively. Plane wave incidence on the Peace Lily plant model, 1 g SAR and 10 g SAR spatial distributions on three dimensional exterior surface of the prototyped Peace Lily plant are illustrated in Figs. 3(a), 3(b), and 3(c), respectively. All these SAR distributions are illustrated in particular at 2450 MHz for the direction of incident wave propagation (plane wave): $x = -1$ and electric field alteration along the y-axis. Looking at the spatial SAR distributions, it is important to mention that enhanced charge accumulation, subsequent localized electric field strength development, and further induced surface current density together occur around curved regions on both conducting bodies with high conductivity (σ) and lossy dielectric objects with reasonable conductivity (σ) [32, 52–54]. Therefore, it is observed that spatial SAR distribution is higher around the curved regions with sudden change in geometry on the prototyped Peace Lily model.

It is precisely recorded that the magnitude of MLP SAR varies 4.18, 4.46, and 6.36 times (i.e., ratio of Max MLP SAR to Min MLP SAR), respectively at 947.50 MHz, 1842.50 MHz, and 2450 MHz owing

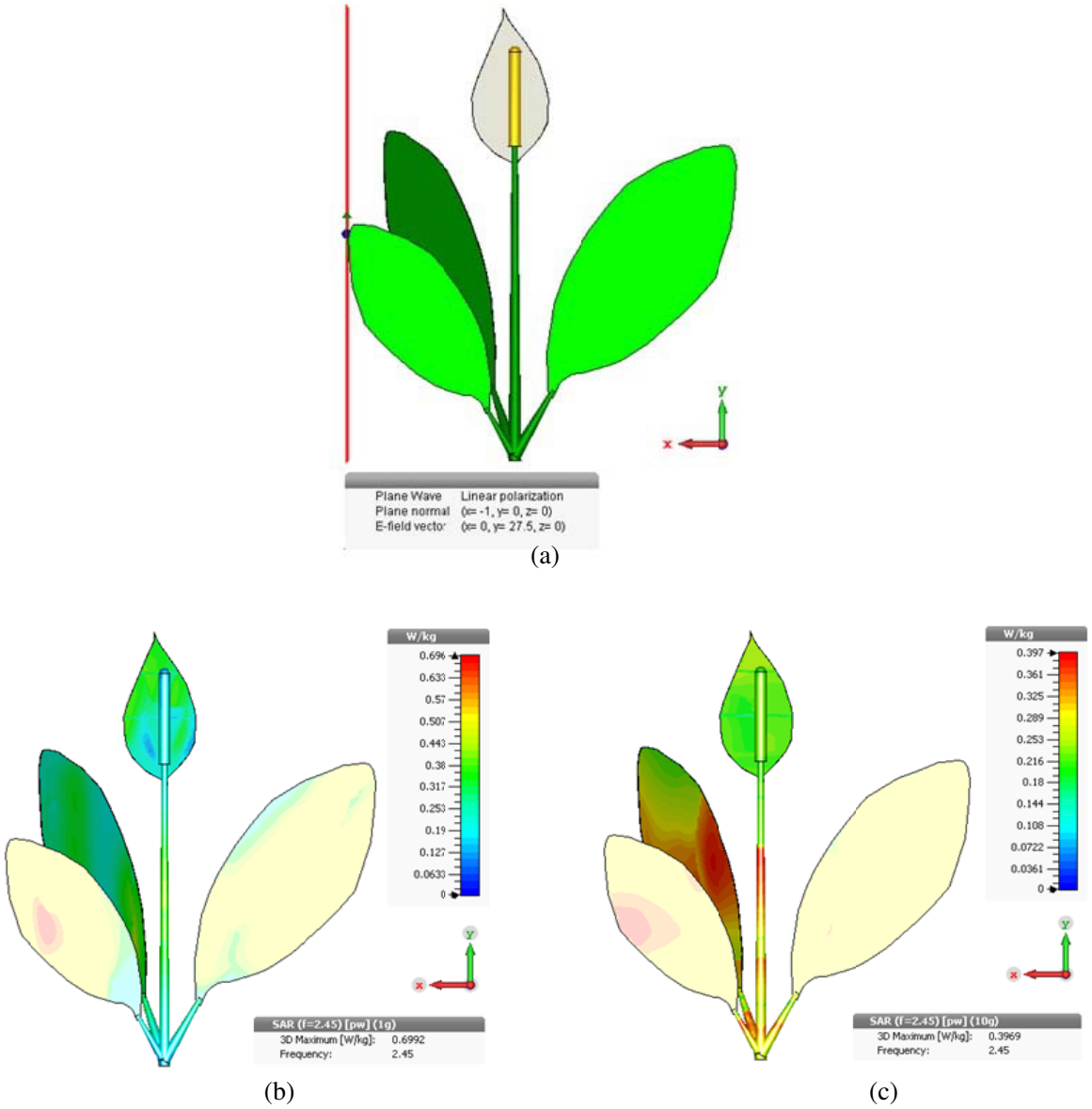

Figure 3. (a) A linearly polarized plane wave has impinged on the Peace Lily model with Direction of Propagation (DoP): $x = -1$ and E field: y axis, (b) corresponding 1 g spatial SAR distribution at 2450 MHz and (c) corresponding 10 g spatial SAR distribution at 2450 MHz.

to six distinct combinations of plane wave direction of arrival and polarization. In this connection, it is noted from Table 3 to Table 5 and Figs. 4(a) to 4(c) that the maximum (or even the minimum) evaluated SAR values at individual frequencies do not arise for the same combination of direction of wave propagation and polarization of incident wave. This observation is similar to earlier reported work available in literature [31, 34]. The wavelength inside tissue material is different at different frequencies of operation — hence, the developed electric field distributions are not the same at different frequencies. SAR value ($\sigma|E|^2/2\rho$) is straightly dependent on the second power of developed electric field magnitude. Therefore, either the maximum or the minimum evaluated SAR values at separate frequencies do not happen to occur for the same combination of propagation direction and wave polarization. Furthermore, even at a specific frequency of operation, the observed spatial coordinates of MLP SAR, maximum 1 g SAR, and maximum 10 g SAR do not overlap with each other. In Table 3 to Table 5, Figs. 4(a) to 4(c),

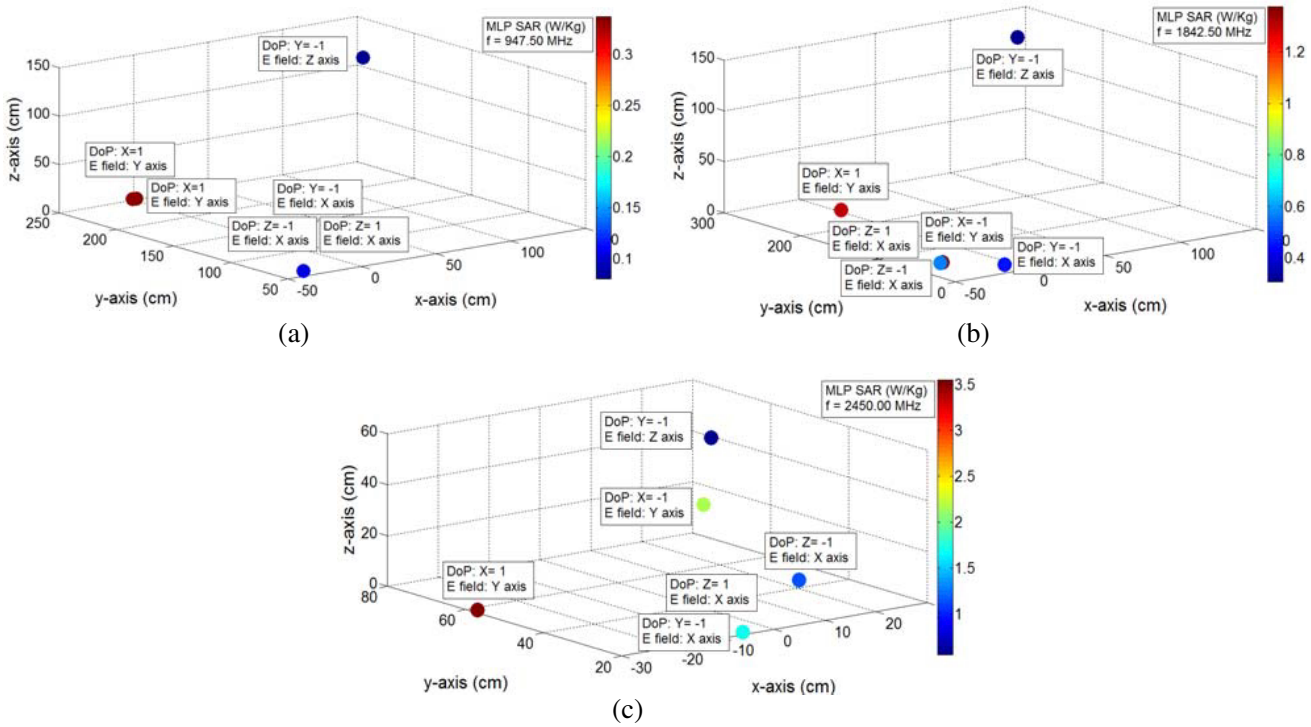

Figure 4. (a) to (c) Contrasts in magnitude and spatial coordinates of MLP SAR for six distinct combinations of direction of arrival and polarization of incident wave at 947.50 MHz, 1842.50 MHz and 2450 MHz.

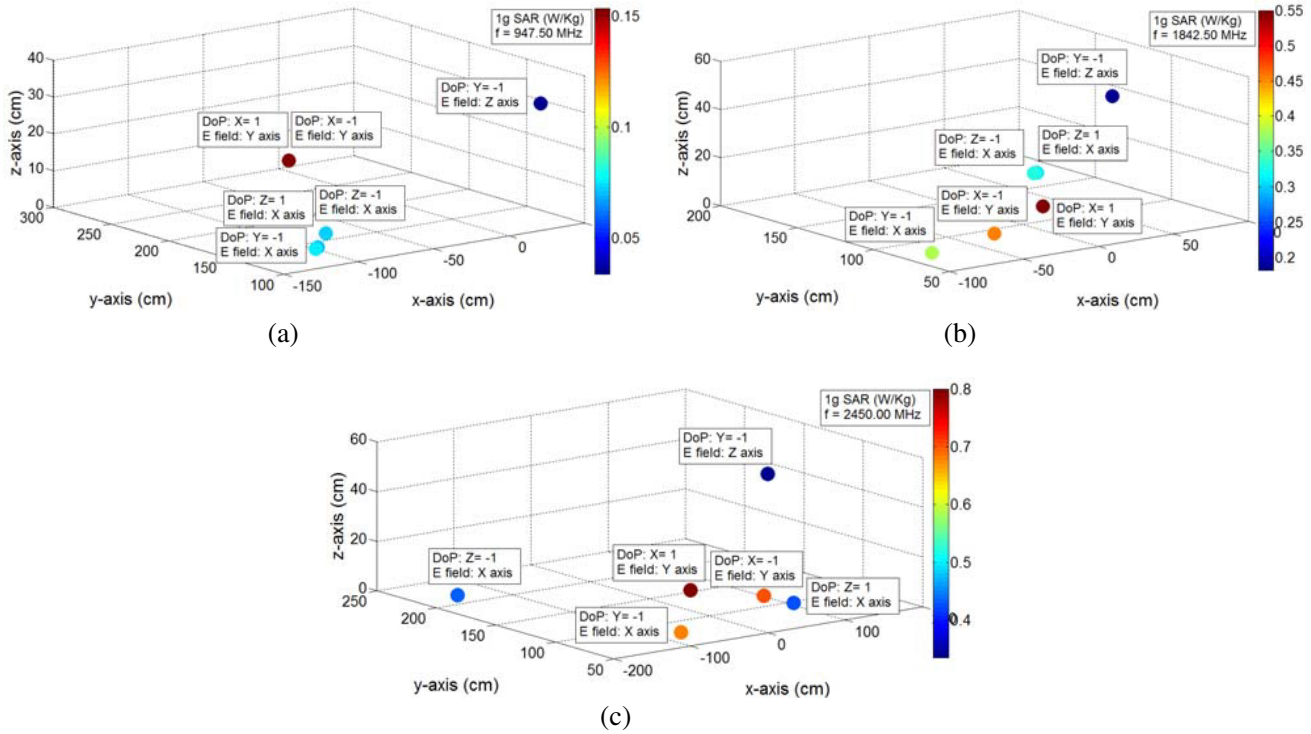

Figure 5. (a) to (c) Contrasts in magnitude and spatial coordinates of 1 g averaged SAR for six distinct combinations of direction of arrival and polarization of incident wave at 947.50 MHz, 1842.50 MHz and 2450 MHz.

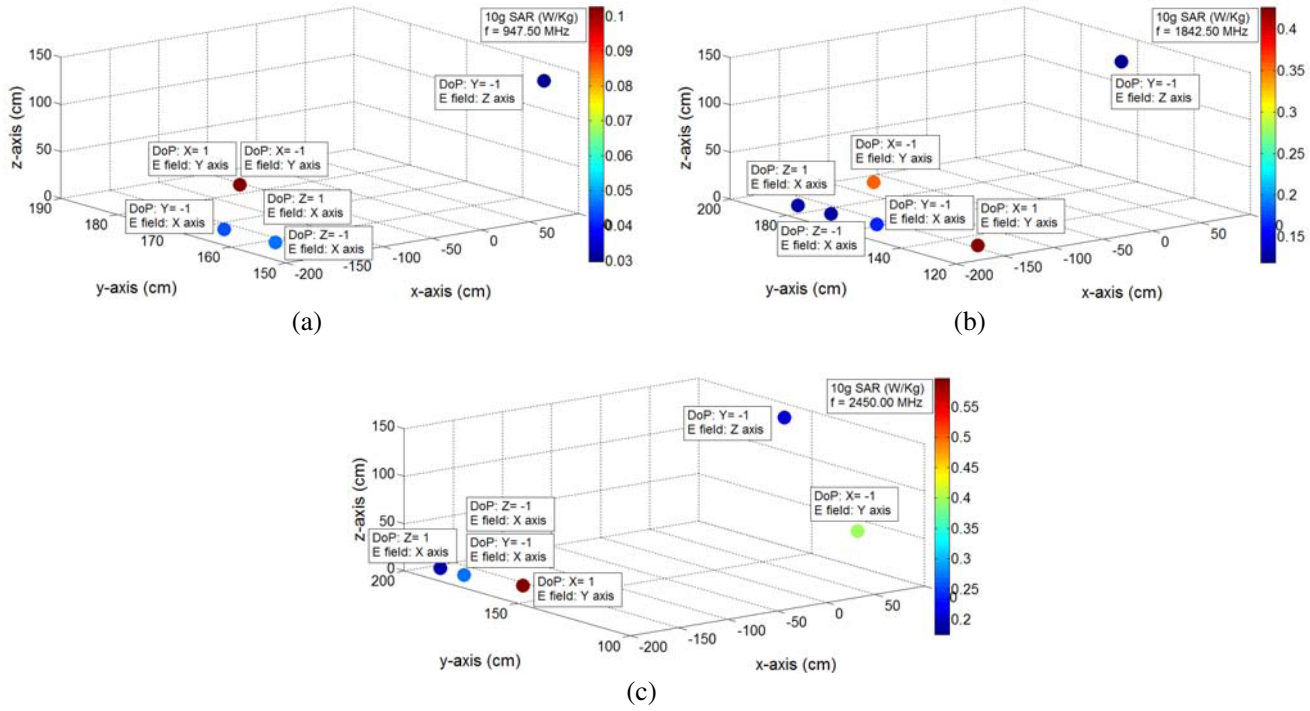

Figure 6. (a) to (c) Contrasts in magnitude and spatial coordinates of 10 g averaged SAR for six distinct combinations of direction of arrival and polarization of incident wave at 947.50 MHz, 1842.50 MHz and 2450 MHz.

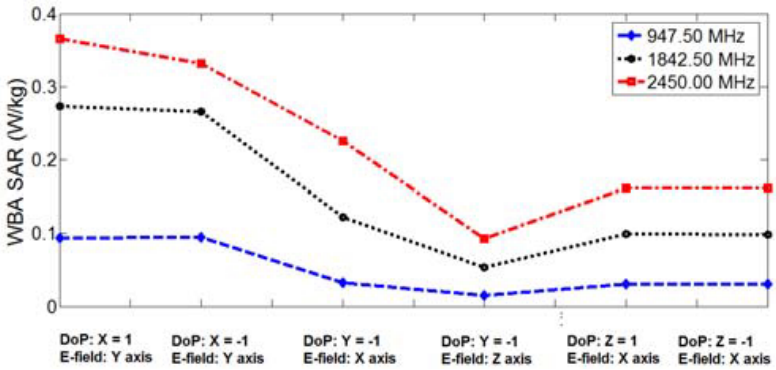

Figure 7. Discrepancies in magnitude of evaluated WBA SAR data at 947.50 MHz, 1842.50 MHz and 2450 MHz.

Figs. 5(a) to 5(c), Figs. 6(a) to 6(c), and Fig. 7, it is evident that there is a wide variation in spatial coordinate location and magnitude of MLP SAR, maximum 1 g averaged SAR, maximum 10 g averaged SAR, and WBA SAR for six distinct combinations of wave propagation direction and polarization at each of the three frequencies. The magnitude of 1 g averaged SAR varies 4.51, 3.02, and 2.39 times (i.e., ratio of Max 1 g averaged SAR to Min 1 g averaged SAR) respectively at 947.50 MHz, 1842.50 MHz, and 2450 MHz for six distinct combinations of direction of wave incidence and polarization. Furthermore, the magnitude of 10 g averaged SAR varies 2.34, 3.60, and 3.40 times (i.e., ratio of Max 10 g averaged SAR to Min 10 g averaged SAR) at 947.50 MHz, 1842.50 MHz, and 2450 MHz, respectively. The WBA SAR varies 6.21, 5.08, and 3.96 folds (i.e., ratio of Max WBA SAR to Min WBA SAR) at the above mentioned three frequencies (refer to Fig. 7).

The designed Peace Lily plant model consists of different dielectric tissue layers; however, the

entire Peace Lily plant model is asymmetric in nature. Thus, six distinct combinations of propagation direction and wave polarization have resulted in 4.18 to 6.36 times alteration in MLP SAR value. Nevertheless for homogeneous fruit model, this variation can be much lower as reported in recent literature [34]. Furthermore, in contrast to earlier reported articles in literature [31, 34], variation in SAR value remains significant even when averaging mass increases. Usually, variation in SAR data in multilayer plant structure is higher than single layer models because of multiple reflections of plane wave at dielectric layer interfaces. As a consequence, localized superposition of incident and reflected waves can result in increased SAR value in multilayer plant model.

Based on the results, it is clear that SAR value significantly varies for the designed Peace Lily plant model due to different directions of wave propagation and wave polarization — even for a particular reference power density level at a particular frequency of operation. Therefore, direct adoption of SAR limit is highly recommended in the revised electromagnetic exposure guidelines — concerned regulatory organizations should take necessary steps without any further delay. However, it should be noted that the Peace Lily plant model can also be designed with varied numbers or orientations of leaves and flowers. As a consequence, the spatial SAR distributions and Max-to-Min SAR ratios can alter to different levels. Strength of this investigation lies in the fact that almost all plant structures are asymmetric in nature, and thus, SAR value for any plant structure will vary based on different directions of wave propagation and wave polarizations. Therefore, the overall observation of SAR data variation for any plant model is generic and applies to almost all plant structures. Though this investigation has been performed as per the existing Indian scenario [41], similar SAR data variations will be observed even in other electromagnetic exposure scenarios [42–46].

6. CONCLUSIONS

Based on the frequency of operation, wave propagation direction of arrival and wave polarization, the spatial coordinates and magnitude of SAR in the Peace Lily plant model alter considerably. It is already known that SAR is largely dependent on geometry, orientation of plant parts, relative positioning of tissue dielectric layers, and plant tissue dielectric properties [27–34]. Furthermore, it is already a known fact that the permittivity (ε'_r) and loss tangent ($\tan\delta$) of different plant tissues change with aging process [55]. Hence, this factor can additionally alter the electric field distribution and SAR distribution in Peace Lily or other plant model. It is evident that even under exactly the same prescribed power density limit, actual SAR value can change severely in the plant model based on the direction of wave incidence and polarization. Thus, the entire SAR estimation in plant and fruit models cannot be directly correlated to the prescribed reference power density limit. This particular work has been conducted considering the existing Indian electromagnetic exposure scenario for general public protection [41]. Nevertheless, different international and national electromagnetic standards do not share uniformity among themselves, thus required to be harmonized [41–48]. It should be noted that to date no organization has ever prescribed electromagnetic exposure regulatory guidelines in particular to protect fruits, flowers, and plants — thus, all SAR data and spatial distributions for the Peace Lily plant model have been evaluated considering Indian public exposure guidelines [41]. Furthermore with the recent deployment of sub-6 GHz 5G telecommunication infrastructure in India and worldwide, SAR data can also be evaluated at additional frequencies such as 2100 MHz, 3500 MHz, and 5200 MHz — considerable variations in highest magnitude and associated spatial coordinates of SAR data are expected for the Peace Lily plant model at those 5G frequencies (sub-6 GHz) due to variations in direction of wave propagation and incident wave polarization. In addition, the work can be further extended to evaluate SAR (or absorbed power density) data at higher frequencies of 5G communication, i.e., at 26 GHz, 28 GHz, or 39 GHz, etc. To this end, directly adopting the SAR limit for plant and fruit model seems necessary and recommended in far field considering the overall scenario — else, limiting the reference power density cannot really ensure a maximum limit on electromagnetic energy absorption rate in plants. However, judicious SAR limit selection to protect plants and fruits is required based on further investigations related to electromagnetic exposure mediated plant responses [56–62] — once finalized, the prescribed SAR limit should not be crossed else plants can suffer from potential biological effects due to electromagnetic exposure. Thus, electromagnetic irradiation induced physiological (such as plant growth and chlorophyll concentrations) and molecular responses (stress sensitive gene expressions)

in Peace Lily and other plants need to be investigated in accordance with Indian as well as other national or international electromagnetic exposure regulatory standards [41–46] — with reference to past studies reported in literature [56–62]. In general, the nutrition value of crops and fruits should also be investigated as they grow under electromagnetic irradiation — the same is associated with human nutrition intake from plants. However, electromagnetic irradiation evoked plant responses should never be correlated with radiation hazards on human health — rather, can be sensibly analyzed to enforce protection for plants, crops, and the entire ecosystem.

ACKNOWLEDGMENT

Authors would like to thank Prof. Bhaskar Gupta, Electronics and Telecommunication Engineering Department, Jadavpur University, India and Mr. Soham Ghosh, research scholar, Electronics and Telecommunication Engineering Department, Jadavpur University, India for their constructive suggestions and support.

REFERENCES

1. Gabriel, C., S. Gabriel, and Y. E. Corthout, "The dielectric properties of biological tissues: I. Literature survey," *Physics in Medicine & Biology*, Vol. 41, No. 11, 2231–2249, 1996.
2. Gabriel, S., R. W. Lau, and C. Gabriel, "The dielectric properties of biological tissues: II. Measurements in the frequency range 10 Hz to 20 GHz," *Physics in Medicine & Biology*, Vol. 41, No. 11, 2251–2269, 1996.
3. Gabriel, S., R. W. Lau, and C. Gabriel, "The dielectric properties of biological tissues: III. Parametric models for the dielectric spectrum of tissues," *Physics in Medicine & Biology*, Vol. 41, No. 11, 22712293, 1996.
4. Nelson, S. O., S. Trabelsi, and A. W. Kraszewski, "Advances in sensing grain moisture content by microwave measurements," *Transactions of the ASAE*, Vol. 41, No. 2, 483–487, 1998.
5. Guo, W., S. O. Nelson, S. Trabelsi, and S. J. Kays, "10–1800 MHz dielectric properties of fresh apples during storage," *J. of Food Engg.*, Vol. 83, No. 4, 562–569, 2007.
6. Nelson, S. O. and S. Trabelsi, "Dielectric spectroscopy measurements on fruit, meat, and grain," *Trans. of the ASABE*, Vol. 51, No. 5, 1829–1834, 2008.
7. Kundu, A. and B. Gupta, "Broadband dielectric properties measurement of some vegetables and fruits using open ended coaxial probe technique," *Proceedings of The 2014 International Conference on Control, Instrumentation, Energy and Communication (CIEC)*, 480–484, IEEE, Kolkata, 2014.
8. Gandhi, O. P., "Yes the children are more exposed to radiofrequency energy from mobile telephones than adults," *IEEE Access*, Vol. 3, 985–988, 2015.
9. Takei, R., T. Nagaoka, K. Saito, S. Watanabe, and M. Takahashi, "SAR variation due to exposure from a smartphone held at various positions near the torso," *IEEE Transactions on Electromagnetic Compatibility*, Vol. 59, No. 2, 747–753, 2017.
10. Yelkenci, T., "Effects of metallic objects on specific absorption rate in the human head for 915 and 1900 MHz mobile phones," *Frequenz*, Vol. 60, Nos. 3–4, 46–50, 2006.
11. Christ, A. K., T. Samaras, C. Goiceanu, and N. Kuster, "The dependence of electromagnetic far-field absorption on body tissue composition in the frequency range from 300 MHz to 6 GHz," *IEEE Transactions on Microwave Theory and Techniques*, Vol. 54, No. 5, 2188–2195, 2006.
12. Yelkenci, T. and S. Paker, "The effects of frequency, polarization, direction and metallic objects on the SAR values in a human head model for plane wave exposure (500–2500 MHz)," *Frequenz*, Vol. 60, Nos. 11–12, 215–219, 2006.
13. Cooper, J. and V. Hombach, "The specific absorption rate in a spherical head model from a dipole with metallic walls nearby," *IEEE Transactions on Electromagnetic Compatibility*, Vol. 40, No. 4, 377–382, 1998.

14. Meier, K., V. Hombach, R. Kastle, R. Y.-S. Tay, and N. Kuster, "The dependence of electromagnetic energy absorption upon human-head modeling at 1800 MHz," *IEEE Transactions on Microwave Theory and Techniques*, Vol. 45, No. 11, 2058–2062, 1997.
15. Mirotznik, M. S., E. Cheever, and K. R. Foster, "High-resolution measurements of the specific absorption rate produced by small antennas in lossy media," *IEEE Transactions on Instrumentation and Measurement*, Vol. 45, No. 3, 754–756, 1996.
16. Kraszewskl, A., M. A. Stuchly, S. S. Stuchly, G. Hartsgrove, and D. Adamski, "Specific absorption rate distribution in a full-scale model of man at 350 MHz," *IEEE Transactions on Microwave Theory and Techniques*, Vol. 32, No. 8, 779–783, 1984.
17. Kaszuba-Zwoińska, J., J. Gremba, B. Gałdzińska-Calik, K. Wójcik-Piotrowicz, and P. J. Thor, "Electromagnetic field induced biological effects in humans," *Przegl. Lek.*, Vol. 72, No. 11, 636–641, 2015.
18. Kıvrak, E. G., K. K. Yurt, A. A. Kaplan, I. Alkan, and G. Altun, "Effects of electromagnetic fields exposure on the antioxidant defense system," *J. Microsc. Ultrastruct.*, Vol. 5, No. 4, 167–176, 2017.
19. Agarwal, A., N. R. Desai, K. Makker, A. Varghese, R. Mouradi, E. Sabanegh, and R. Sharma, "Effects of radiofrequency electromagnetic waves (RF-EMW) from cellular phones on human ejaculated semen: An in vitro pilot study," *Fertil. Steril.*, Vol. 92, No. 4, 1318–1325, 2009.
20. Lewicka, M., G. A. Henrykowska, K. Pacholski, J. Śmigielski, M. Rutkowski, M. Dziedziczak-Buczyńska, and A. Buczyński, "The effect of electromagnetic radiation emitted by display screens on cell oxygen metabolism — in vitro studies," *Arch. Med. Sci.*, Vol. 11, No. 6, 1330–1339, 2015.
21. Lu, Y. S., B. T. Huang, and Y. X. Huang, "Reactive oxygen species formation and apoptosis in human peripheral blood mononuclear cell induced by 900 MHz mobile phone radiation," *Oxid Med. Cell Longev.*, Article ID 740280, 2012.
22. De Iuliis, G. N., R. J. Newey, B. V. King, and R. J. Aitken, "Mobile phone radiation induces reactive oxygen species production and DNA damage in human spermatozoa in vitro," *PLoS One*, Vol. 4, No. 7, 2009 (Erratum in: *PLoS One*, Vol. 8, No. 3, 2013.).
23. Sefidbakht, Y., A. A. Moosavi-Movahedi, S. Hosseinkhani, F. Khodagholi, M. Torkzadeh-Mahani, F. Foolad, and R. Faraji-Dana, "Effects of 940 MHz EMF on bioluminescence and oxidative response of stable luciferase producing HEK cells," *Photochem. Photobiol. Sci.*, Vol. 13, No. 7, 1082–1092, 2014.
24. Behari, J., "Biological responses of mobile phone frequency exposure," *Indian J. Exp. Biol.*, Vol. 48, No. 10, 959–981, 2010.
25. Duhaini, I., "The effects of electromagnetic fields on human health," *Physica Medica*, Vol. 32, No. 3, 213, 2016.
26. Hu, C., H. Zuo, and Y. Li, "Effects of radiofrequency electromagnetic radiation on neurotransmitters in the brain," *Frontiers in Public Health*, Vol. 9, 1–15, Article ID 691880, 2021.
27. Kundu, A. and B. Gupta, "Comparative SAR analysis of some Indian fruits as per the revised RF exposure guideline," *IETE Journal of Research*, Vol. 60, No. 4, 296–302, 2014.
28. Kundu, A., "Specific absorption rate evaluation in apple exposed to RF radiation from GSM mobile towers," *2013 IEEE Applied Electromagnetics Conference (AEMC)*, 1–2, IEEE, Bhubaneswar, India, 2013.
29. Kundu, A., B. Gupta, and A. I. Mallick, "SAR analysis in a typical bunch of grapes exposed to radio frequency radiation in Indian scenario," *2016 International Conference on Microelectronics, Computing and Communications (MicroCom)*, 1–5, IEEE, 2016.
30. Kundu, A., B. Gupta, and A. I. Mallick, "Specific absorption rate evaluation in a typical multilayer fruit: Coconut with twig due to electromagnetic radiation as per Indian standards," *Microwave Review (Mikrotalasana Revija)*, Vol. 23, No. 2, 24–32, 2017.
31. Kundu, A., B. Gupta, and A. I. Mallick, "Dependence of electromagnetic energy distribution inside a typical multilayer fruit model on direction of arrival and polarization of incident field," *2019 IEEE Radio and Antenna Days of the Indian Ocean (RADIO)*, 1–2, IEEE, 2019.

32. Kundu, A., B. Gupta, and A. I. Mallick, "Contrast in specific absorption rate for a typical plant model due to discrepancy among global and national electromagnetic standards," *Progress In Electromagnetics Research M*, Vol. 99, 139–152, 2021.
33. Kundu, A., B. Gupta, and A. I. Mallick, "Estimation of specific absorption rate levels in a typical fruit specimen and observations on their variations according to different electromagnetic standards," *Microwave Review*, Vol. 27, No. 2, 2021.
34. Kundu, A., B. Gupta, and A. I. Mallick, "Dependence of specific absorption rate and its distribution inside a homogeneous fruit model on frequency, angle of incidence, and wave polarization," *Frequenz*, Vol. 76, Nos. 1–2, 109–119, 2022.
35. Deschamps, G., "Impedance of an antenna in a conducting medium," *IRE Trans. Antennas and Propagation*, Vol. 10, No. 5, 648–650, 1962.
36. Liu, L., D. Xu, and Z. Jiang, "Improvement in dielectric measurement technique of open-ended coaxial line resonator method," *Electronics Letters*, Vol. 22, No. 7, 373–375, 1986.
37. Xu, D., L. Liu, and Z. Jiang, "Measurement of the dielectric properties of biological substances using an improved open-ended coaxial line resonator method," *IEEE Transactions on Microwave Theory and Techniques*, Vol. 35, No. 12, 1424–1428, 1987.
38. Stuchly, M. A. and S. S. Stuchly, "Coaxial line reflection method for measuring dielectric properties of biological substances at radio and microwave frequencies — A review," *IEEE Trans. Instrum. Meas.*, Vol. 29, No. 3, 176–183, 1980.
39. Athey, T. W., M. A. Stuchly, and S. S. Stuchly, "Measurement of radio frequency permittivity of biological tissues with an open-ended coaxial line: Part I," *IEEE Transactions on Microwave Theory and Techniques*, Vol. 30, No. 1, 82–86, 1982.
40. CST STUDIO SUITE 2016, https://www.3ds.com/products-services/simulia/products/cst-studio-suite/.
41. DoT, *Mobile Communication — Radio Waves & Safety*, 1–15, India, 2012.
42. ICNIRP, "Guidelines for limiting exposure to electromagnetic fields (100 kHz to 300 GHz)," *Health Phys.*, Vol. 118, No. 5, 483–524, 2020.
43. Cleveland, Jr., R. F., D. M. Sylvar, and J. L. Ulcek, "Evaluating compliance with FCC guidelines for human exposure to radiofrequency electromagnetic fields," *FCC OET Bulletin*, Vol. 65, Edition 97-01, Washington D.C., 1997.
44. SAEFL, *Electrosmog in the Environment*, 1–56, Switzerland, 2005.
45. Ministry of Health of the Russian Federation, "SanPiN 2.1.8/2.2.4.1190-03: Arrangement and operation of land mobile radiocommunication facilities — Hygienic requirements," 1–17, Russia, 2003.
46. The president of the council of ministers (Italy), "Establishment of exposure limits, attention values, and quality goals to protect the population against electric, magnetic, and electromagnetic field generated at frequencies between 100 kHz and 300 GHz (unofficial translation by P. Vecchia)," 1–6, Italy, 2003.
47. Vecchia, P., "Radiofrequency fields: Bases for exposure limits," *2 European IRPA Congress on Radiation Protection — Radiation Protection: From Knowledge to Action*, 1–19, Paris, 2006.
48. Foster, K. R., "Exposure limits for radiofrequency energy: Three models," *Proceedings of the Eastern European Regional EMF Meeting and Workshop (Criteria for EMF Standards Harmonization)*, 1–6, Varna, Bulgaria, 2001.
49. Weiland, T., "A discretization method for the solution of Maxwell's equations for six-component fields," *Electronics and Communications AEU*, Vol. 31, No. 3, 116–120, 1977.
50. Clemens, M. and T. Weiland, "Discrete electromagnetism with the finite integration technique," *Progress In Electromagnetics Research*, Vol. 32, 65–87, 2001.
51. "IEC/IEEE International Standard — Determining the peak spatial-average specific absorption rate (SAR) in the human body from wireless communications devices, 30 MHz to 6 GHz — Part 1: General requirements for using the finite-difference time-domain (FDTD) method for SAR calculations," *IEC/IEEE 62704-1: 2017*, 1–86, United States, 2017.

52. Bhattacharya, K., "On the dependence of charge density on surface curvature of an isolated conductor," *Physica Scripta*, Vol. 91, No. 3, 035501, 2016.
53. Jordan, E. C. and K. G. Balmain, *Electromagnetic Waves and Radiating Systems*, 2nd Edition, PHI Learning, New Delhi, 2009.
54. Deshpande, M. D., C. R. Cockrell, F. B. Beck, E. Vedeler, and M. B. Koch, "Analysis of electromagnetic scattering from irregularly shaped, thin, metallic flat plates," *NTRS — NASA Technical Reports Server*, NASA Technical Paper 3361, 1993.
55. Kataria, T. K., J. L. Olvera-Cervantes, A. Corona-Chávez, R. Rojas-Laguna, and M. E. Sosa-Morales, "Dielectric properties of guava, mamey sapote, prickly pears, and Nopal in the microwave range," *International Journal of Food Properties*, Vol. 20, No. 12, 2944–2953, 2017.
56. Vian, D. R., S. Girard, P. Bonnet, F. Paladian, E. Davies, and G. Ledoigt, "Microwave irradiation affects gene expression in plants," *Plant Signaling & Behavior*, Vol. 1, No. 2, 67–69, 2006.
57. Roux, D., A. Vian, S. Girard, P. Bonnet, F. Paladian, E. Davies, and G. Ledoigt, "Electromagnetic fields (900 MHz) evoke consistent molecular responses in tomato plants," *Physiologia Plantarum*, Vol. 128, No. 2, 283–288, 2006.
58. Roux, D., C. Faure, P. Bonnet, S. Girard, G. Ledoigt, E. Davies, M. Gendraud, F. Paladian, and A. Vian, "A possible role for extra-cellular ATP in plant responses to high frequency, low amplitude electromagnetic field," *Plant Signaling & Behavior*, Vol. 3, No. 6, 383–385, 2008.
59. Vian, A., C. Faure, S. Girard, E. Davies, F. Hallé, P. Bonnet, G. Ledoigt, and F. Paladian, "Plants respond to GSM like radiations," *Plant Signaling & Behavior*, Vol. 2, No. 6, 522–524, 2007.
60. Vian, A., E. Davies, M. Gendraud, and P. Bonnet, "Plant responses to high frequency electromagnetic fields," *BioMed Research International*, Article ID 1830262, 2016.
61. Kundu, A., S. Vangaru, S. Bhattacharyya, A. I. Mallick, and B. Gupta, "Electromagnetic irradiation evokes physiological and molecular alterations in rice," *Bioelectromagnetics*, Vol. 42, No. 2, 173–185, 2021.
62. Kundu, A., S. Vangaru, S. Bhowmick, S. Bhattacharyya, A. I. Mallick, and B. Gupta, "One-time electromagnetic irradiation modifies stress-sensitive gene expressions in rice plant," *Bioelectromagnetics*, Vol. 42, No. 8, 649–658, 2021.